Int. J. Heat Mass Transfer. Vol. 27, No. 8, pp. 1379–1394, 1984
Printed in Great Britain

0017–9310/84 $3.00 + 0.00

HEAT TRANSFER DURING A SMALL-BREAK LOSS-OF-COOLANT ACCIDENT IN A PRESSURIZED WATER REACTOR—A PARAMETRIC STUDY FOR A 4 in. LOWER-PLENUM BREAK

NIKOS C. MARKATOS
Computational Fluid Dynamics Unit, Imperial College, London SW7 2BX, U.K.

and

STEPHEN M. RAWNSLEY and D. BRIAN SPALDING*
Concentration Heat and Momentum Limited, Bakery House, 40 High Street, Wimbledon, London SW19 5AU, U.K.

(*Received* 17 *February* 1983 *and in revised form* 12 *October* 1983)

Abstract—A major safety concern in pressurized-water-reactor (PWR) design is the loss-of-coolant accident (LOCA), in which a break in the primary coolant circuit leads to depressurization, boiling of the coolant, consequent reduced cooling of the reactor core, and, unless remedial measures are taken, overheating of the fuel rods. This concern has led to the development of several computer models for safety analysis, the validity of which can be assessed only after their accuracy and sensitivity have been subjected to parametric studies, such as: nodalization studies to ensure grid-independency of the results; investigation of alternative empirical input, such as heat-transfer representations, choice of flow regimes, etc., and the representation of stratified two-phase flow in the horizontal pipes. This paper presents such parametric studies for a postulated PWR accident. The results are presented and discussed. It is concluded that the predictions are significantly affected by the number of grid nodes used, by the chosen heat-transfer and interphase friction correlations and by the modelling of stratified two-phase flow in horizontal pipes. Such sensitivities may, it is suggested, be exhibited by other LOCA simulations.

NOMENCLATURE

A_{ip}	interface area
A_l	liquid cross-sectional area
A_{wall}	pipe curved surface area
A_{wi}	pipe surface area in contact with phase i
C	interphase heat transfer coefficient
$C_{f,ip}$	interphase friction coefficient
C_p	isobaric specific heat
f	friction factor
F	wall friction force
F_{ip}	interphase friction force per cell
F_s	liquid momentum source term
g	gravitational acceleration
h	specific enthalpy
h_{lg}	latent heat of vaporization
K	thermal conductivity
$\dot{m}_{lg}$	interphase mass transfer rate per cell
P_h	hydrostatic pressure
$\dot{q}$	heat transfer rate
Q_{chf}	critical heat flux
r	pipe radius
R	volume fraction
S_ϕ	source term
T	temperature
T_{min}	minimum film-boiling temperature
T_{nh}	homogeneous nucleation temperature
T_{sat}	saturation temperature
u	velocity.

Greek symbols

θ	half-angle subtended at the centre of the horizontal pipes by the vapour–liquid interface
ρ	density
σ	surface tension
ϕ	dependent variable.

Subscripts

g	vapour
gi	vapour-to-fluid interface
i	vapour or liquid
l	liquid
li	liquid-to-fluid interface
sat	saturation.

* Present address: Faculty of Science and Mathematics, Thames Polytechnic, London SE18 6PF, U.K.

1. INTRODUCTION

1.1. *The problem considered*

STUDIES of the transient behaviour of a pressurized water reactor (PWR) are required over a wide range of accident conditions for predicting the possibility of fuel-rod failure and, hence, for the design of adequate safety systems. Most of the analytical development effort over the past 15 years has been devoted to the large-break loss-of-coolant accident (LOCA). The accident at Three-Mile Island, however, has resulted in an increased priority for analyses that deal with the much longer transients that ensue from smaller leaks.

With the above in mind, the problem considered in this work is a 4 in. diameter small break in the reactor lower plenum, although the same analysis can also be used for other postulated accidents. The 4 in. break is much greater than the maximum size which is assumed possible to occur in the reactor plenum, but this LOCA enables the heat-transfer and friction correlations to be studied over a wide range of flow conditions.

1.2. *Previous work and present contribution*

Analysis has played a significant role in nuclear reactor safety since full-scale experiments (or actual

events) are neither available nor practical to obtain; and extrapolation of the results of tests on scaled-down systems to the actual reactor system is difficult. Therefore, the development of analytical methods for safety analysis has been receiving serious attention over the past 15 years. An excellent review of existing analytical capabilities is given in ref. [1]; it shows that few sensitivity analyses, either of numerical or physical influences on the predictions, have been reported so far.

The present study involves the application of the LAURA (loop analysis of unsteady reactor flows) program [2] to a typical small-break LOCA, with a view of demonstrating the importance of the above-mentioned sensitivity studies. In particular, the purpose of the reported work is to investigate three influences on the predictions:

(a) The effect of the fineness of the nodalization of the reactor circuit.

(b) The effects of the representation of interphase heat transfer and interphase friction processes.

(c) The effect of stratified two-phase flow in the horizontal pipes, with the possibility of counter-current flow.

LAURA embodies a full two-fluid model, and therefore is capable of handling nonhomogeneous, nonequilibrium effects.

It also has the capability to represent the detailed friction and heat-transfer processes through formulae chosen by the user. In this study, the formulae are mainly those which are to be found in other more widely-used codes namely TRAC [3], RELAP [4], and REFLUX [5].

2. DESCRIPTION OF THE PROBLEM

The system considered is a typical 3500 MW 4-loop plant, subjected to a depressurization caused by a 4 in. (102 mm) diameter hole in the lower plenum of the reactor vessel. It is assumed that the four loops of the primary circuit behave identically,† and may be considered as a single loop for the purposes of analysis. This loop is divided into a number of regions that are connected by flow paths. Each region is further subdivided into a number of control volumes, for the purposes of the finite-domain solution procedure. The configuration of the single-loop circuit and the model region-diagram are shown in Fig. A1. The definitions of each of the 14 regions shown, together with the main dimensions are given in Appendix 1, together with the accident-event sequence.

No claim is being made here, it should be emphasized, that any particular PWR system is well represented by this model. All that is desired is sufficient typicality that the conclusions about sensitivities will have practical relevance.

† A reviewer of this paper has correctly pointed out that this assumption represents a departure from actual PWR practice. However, there is no reason to suppose that this departure invalidates the general conclusions which can be drawn.

3. THE MATHEMATICAL REPRESENTATION

3.1. *The differential equations*

The independent variables of the problem are the distance around the circuit (x) and the time (t).

The main dependent variables are: steam and water volume fractions, R_g and R_l; steam and water velocities, u_g and u_l; pressure, p; and steam and water enthalpies, h_g and h_l. The governing equations for all dependent variables above can be expressed in the following standard form

$$\frac{\partial}{\partial t}(\rho_i R_i \phi) + \frac{\partial}{\partial x}(\rho_i R_i u_i \phi) = S_\phi, \tag{1}$$

where ϕ and S_ϕ stand for the dependent variable and the source terms, respectively; and subscript i refers to the phase in question.

In addition to the above equations, a two-dimensional conduction equation is solved to allow the calculation of the rod-temperature variations both in the axial direction and across the radius of a rod. The modelling allows for three distinct regions, namely fuel-rod, gap and clad; therefore, a total of eight differential equations are solved in the present investigation. Donor-flux differencing is used, and the equations are cast in fully-implicit form, both ensuring unconditional stability.

3.2. *The stratification model*

The realistic representation of stratified flow requires the effect of interface level variations to be accounted for in addition to including realistic interphase friction correlations. The behaviour of the flow in the horizontal pipes may be significantly affected by the associated hydrostatic pressure gradients, which may induce wave motion along the pipes. Since these pressure gradients are normal to the direction of flow they cannot be resolved by a one-dimensional code, which can only calculate pressure variations in the flow direction. To produce these gravitational effects on the liquid an additional term was included in the liquid momentum equation, of the form

$$F_s = \int_{A_l} p_h \, dA_l, \tag{2}$$

where F_s is the momentum source term for the liquid velocity (N); A_l is the pipe cross-sectional area filled by water; and p_h is the radially varying hydrostatic pressure.

The assumed flow pattern for a varying interface level is shown, for two control volumes, in Fig. A2(a). Then, it can be shown (Appendix 2) that the net force acting on the momentum control volume, due to the interface level variation, is given by

$$F_s = (\rho_l - \rho_g)\frac{gr^3}{6}(6\theta_1 - 6\theta_2 - 3\sin\theta_1 + 3\sin\theta_2 - 3\sin 2\theta_1 + 3\sin 2\theta_2 + \sin 3\theta_1 - \sin 3\theta_2), \tag{3}$$

where $2\theta_1$ and $2\theta_2$ are the angles subtended at the centre

of the pipe by the liquid level, at nodes 1, 2, respectively. Consideration of the pipe cross-sectional area filled by liquid yields

$$2\theta - \sin 2\theta = 2\pi R_l. \tag{4}$$

θ is calculated by a Newton–Raphson iteration using equation (4) and therefore all terms in equation (3) are known.

Allowances are made for the ends of the hot-leg pipe where, for instance, it enters the reactor upper plenum. A collapsed-liquid level is calculated for the upper plenum to determine whether or not the hot-leg pipe is above, below or around that level, and therefore to calculate a stratification term for the pipe-to-plenum liquid velocity. No such allowance is made for the cold-leg pipe.

3.3. *Boundary conditions and physical properties*

The boundary conditions for the circuit (e.g. treatment of pressurizer, ECCS, reactor upper-head and break) and the physical properties are as given in Appendix 3, together with the core heat generation and steam generator heat transfer.

3.4. *Wall friction and pressure drops*

The wall friction force, F_i, acting on each phase is given by

$$F_i = 0.5\rho_i f u_i^2 A_{wi},$$

where

$$f = 0.079Re^{-0.25}, \quad Re \geqslant 2000, \tag{5}$$

$$= 16/Re, \quad Re < 2000, \tag{6}$$

and A_{wi} is the wall surface area in contact with phase i. For uniformly dispersed phases

$$A_{wi} = R_i A_{wall}, \tag{7}$$

where R_i is the phase $-$i volume fraction, and A_{wall} is the total wall surface area.

For regions of stratified flow an estimate of the wall–liquid contact area is derived from equations (4) and (8)

$$A_{wl} = \frac{\theta}{\pi} A_{wall}. \tag{8}$$

Then

$$A_{wg} = A_{wall} - A_{wl}. \tag{9}$$

Losses due to expansions and contractions are treated as in RELAP [4] and in ref. [2].

3.5. *Heat transfer between fuel rods and fluid*

Correlations to be found in the RELAP4/MOD6, TRAC and REFLUX codes have been adapted for use by LAURA. The flow regimes are determined by both cladding temperature and local void fraction, as shown in Table 1.

The critical-heat-flux temperature, T_{chf}, is calculated

Table 1. Flow regimes

Void fraction				
1.0	Convection to single-phase liquid	Forced-convection annular flow	Transition boiling (high quality)	Dispersed flow
0.2		Nucleate boiling	Transition boiling (low quality)	Inverse-annular film boiling
0.0				
		T_{sat}	T_{chf}	T_{min} Wall temperature

from the critical-heat-flux, Q_{chf}, and Chen's nucleate boiling coefficient. The critical heat flux is obtained from Zuber (modified)

$$Q_{chf} = 0.131 R_l \rho_g h_{lg} \left(\frac{\sigma g (\rho_l - \rho_g)^{0.25}}{\rho_g^2} \right). \tag{10}$$

The minimum-film-boiling temperature, T_{min}, is calculated from the homogeneous nucleation correlation, used in TRAC

$$T_{min} = T_{nh} + (T_{nh} - T_l) A^{0.5}, \tag{11}$$

where

$$A = \frac{(K\rho C_p)_l}{(K\rho C_p)_{wall}}, \tag{12}$$

and T_{nh} is the homogeneous nucleation temperature, taken to be the critical temperature (647.3 K) as in TRAC. The set of correlations used in the present calculations is that used in REFLUX [5]. The correlations used for each flow regime are outlined in Table 2.

3.6. *Interphase friction*

In the present investigation, two of the most widely used sets of correlations were used, namely, those of RELAP4/MOD6 [4] and of TRAC [3]. The form in

Table 2. Core solid–fluid heat-transfer correlations

Regime	Correlation	
	Vapour	Liquid
Single-phase vapour	Dittus–Boelter	—
Dispersed	Dittus–Boelter	Radiation
Inverted-annular	Bromley	Radiation
Transition (high quality)	Dittus–Boelter	Log–log interpolation
Transition (low quality)	Bromley	
Nucleate, forced-convection annular	—	Chen
Single-phase liquid	—	Dittus–Boelter
Critical heat flux	Zuber (modified)	
Minimum film boiling temperature	Homogeneous nucleation	

which those correlations were used is given in detail in ref. [2].

Various representations of interphase friction have been used in the stratified-flow regions, the hot- and cold-leg pipes. These representations are:

(1) Homogeneous flow, for which the setting of $C_{f,ip} = 10^{10}$ in the following equation for the interphase friction force F_{ip} results in negligible slip

$$F_{ip} = C_{f,ip} R_g R_l |u_g - u_l| \times \text{cell volume}. \quad (13)$$

(2) A constant value of $C_{f,ip} = 10^3$, which is representative of the magnitude obtained in regions of droplet flow.

(3) An empirical correlation for the interphase friction factor, f, by Ellis and Gay [6] where

$$f = 1.292(Re_{vapour})^{-0.57}, \quad (14)$$

and

$$F_{ip} = 0.5\rho_g f(u_g - u_l)^2 A_{wall} \frac{\sin\theta}{\pi}. \quad (15)$$

Representation (3) assumes a complete separation of phases; and, strictly speaking, equation (14) is only valid for smooth interfaces. The equivalent value for $C_{f,ip}$ is of the order of zero to unity, allowing considerable slip and countercurrent flow.

3.7. *Interphase heat and mass transfer*

The interphase heat-transfer rates are evaluated from the relations

$$\dot{q}_{li} = C_{li} R_g R_l (h_l - h_{l,sat}) \times \text{cell volume}, \quad (16)$$

$$\dot{q}_{gi} = C_{gi} R_g R_l (h_g - h_{g,sat}) \times \text{cell volume}, \quad (17)$$

where $\dot{q}_{li}$ and $\dot{q}_{gi}$ are the rates of heat transfer (W) from the liquid and from the vapour to the interface between the phases.

Prescribing values of 100.0 and 5×10^4 to C_{gi} and C_{li}, respectively, leads to negligible superheating, closely approximating an equal-temperature-of-phase models such as in RELAP4. Reducing the values of C_{gi} and C_{li} leads to thermal non-equilibrium.

The rate of interphase mass transfer in a cell is evaluated from a heat balance at the vapour–liquid interface, using equations (16) and (17). This gives the following expression for the rate of mass transfer from liquid to vapour

$$\dot{m}_{lg} = R_l R_g [C_{li}(h_l - h_{l,sat}) + C_{gi}(h_g - h_{g,sat})] \times \frac{\text{cell volume}}{h_{lg}}. \quad (18)$$

In addition to the simple formulation described above LAURA is also equipped with the relations used in TRAC-PD2 [7].

4. PRESENTATION AND DISCUSSION OF THE RESULTS

4.1. *Computations performed*

A number of separate runs were made for 450 s of the transient, to investigate the sensitivity of the predictions to the interphase-friction representation, to thermal non-equilibrium between the phases, and to the representation of stratified flow in the horizontal pipes. In addition, the effect of grid fineness has been investigated. These runs are summarized in Table 3.

The slip velocities for Run 1 were prescribed to be those given by RELAP4/MOD6 correlations [2]. This required calculation of the interphase friction coefficients considering all the terms in the two momentum equations. An alternative approach was used for Run 2, in which the interphase friction coefficients were deduced from the RELAP4/MOD6 slip correlations using the assumptions of a drift-flux model, of the kind used in RELAP4. In this case many terms are neglected in the momentum equations, i.e. transient, inertia, wall friction, and interphase momentum transfer terms due to interphase mass transfer. Run 3 used the RELAP4 churn-turbulent and homogeneous regimes only, and Run 4 used the correlations for the vessel module of TRAC [2].

Various assumptions for the two-phase flow in the hot- and cold-leg pipes were investigated in Runs 5–8,

Table 3. Computations performed

Run number	Nodes	Interphase-friction coefficients	Non-standard characteristics
1	54	Prescribed RELAP4/MOD6 slip velocity	
2	54	Full RELAP4/MOD6 correlations	
3	54	Partial RELAP4/MOD6 correlations	
4	54	TRAC correlations	
5	54	TRAC correlations	Zero slip in hot- and cold-leg pipes
6	54	TRAC correlations	$C_{f,ip} = 10^3$ in hot- and cold-leg pipes
7	54	TRAC correlations	$C_{f,ip} \simeq 0$ in hot- and cold-leg pipes
8	54	TRAC correlations	$C_{f,ip} \simeq 0$ and gravity in horizontal pipes
9	54	TRAC correlations	As Run 8, and thermal non-equilibrium
10	20	$C_{f,ip} = 10^4$ everywhere	Core rod-to-fluid heat transfer as in ref. [2]
11	37		
12	54		
13	88		
14	156		
15	72		

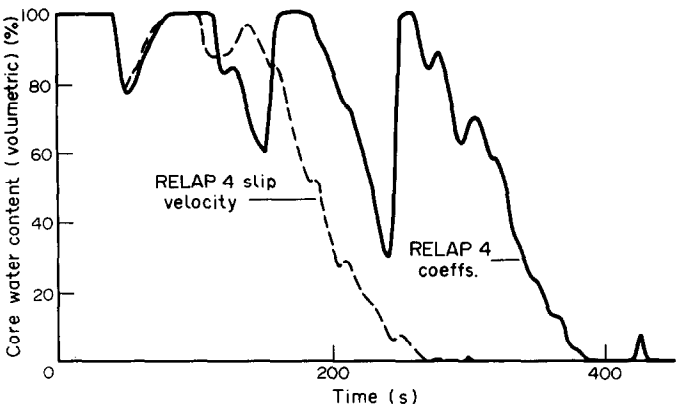

FIG. 1. Core water content for fixed slip and computed slip.

as described in Section 3.7. Each case used the TRAC interphase friction correlations in the remainder of the circuit. Run 8 included the effects of gravity in the horizontal pipes.

The interphase heat-transfer coefficients in Run 9 were reduced by an order of magnitude, giving significant thermal non-equilibrium between the phases, of about 5–10°C. The interphase friction and stratification representations were as for Run 8.

The description of a typical calculation has been reported previously [2] so, for economy of space, the following discussions will concentrate only on describing the effects revealed by the parametric studies performed. The effects of interphase-friction representation (Runs 1–4) are discussed in Section 4.2, the stratification study (Runs 5–8) is described in Section 4.3, and the effects of thermal non-equilibrium (Runs 8 and 9) are discussed in Section 4.4. Finally, the grid-refinement investigation (Runs 10–15) is discussed in Section 4.5.

4.2. *Effect of interphase friction*

The predicted time histories of core water content and mid-core cladding temperatures, respectively, for Runs 1 and 2 are shown in Figs. 1 and 2. Comparison of these calculations enables information to be obtained regarding the application of interphase friction correlations obtained from steady-state experiments, to transient LOCA conditions. It was found that the prescription of the RELAP4/MOD6 slip velocity in the cold side of the steam generators required an unphysical, negative, interphase friction coefficient. To avoid this unrealistic effect the prescribed-slip calculation (Run 1) was performed using the RELAP4 interphase-friction coefficients in the steam generators, and prescribing the slip velocities in the rest of the circuit.

The first 100 s or so of the transient show the same initial voiding, due to saturated conditions being reached after about 45 s, and recovering of the core in each case (Fig. 1). However, substantially different behaviour occurs subsequently. The computed-slip results (Fig. 1, solid line) show periodic uncovering and recovering of the core until complete core uncovering after 390 s. The rapid core recovering for this case after 240 s is due to a plug of liquid present in the hot side of the steam generators, being pushed over to the cold side. This allows rapid circulation of water and steam from the steam generators, through the cold-leg pipe into the reactor, recovering the core from below. The calculation using prescribed interphase slip (Run 1) exhibits a steady uncovering of the core during the period 140–270 s, and the core is constrained by the prescribed slip velocities to remain empty of water, until the end of the calculation after 450 s.

For these cases the greatest cladding temperatures

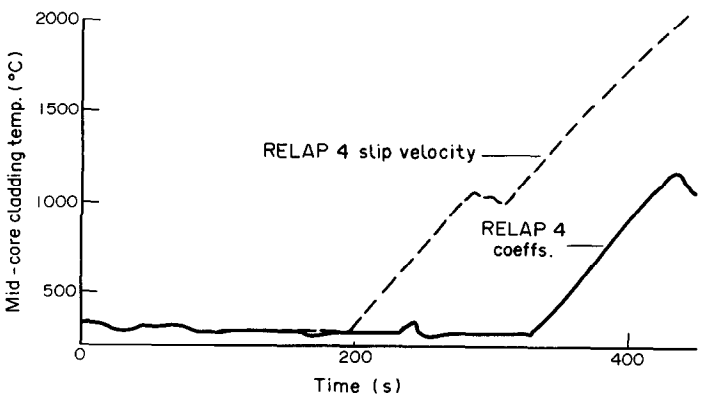

FIG. 2. Mid-core cladding temperature for fixed slip and computed slip.

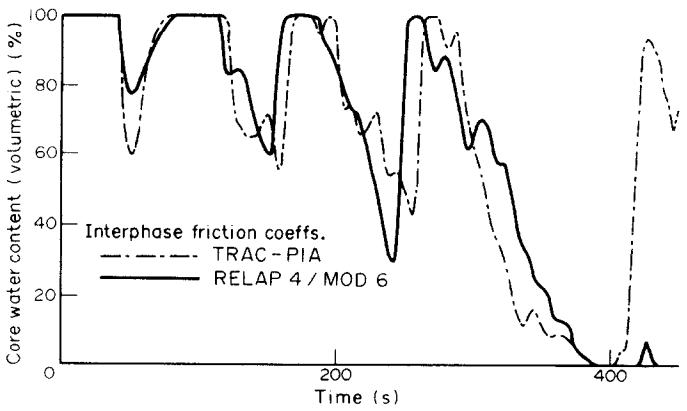

FIG. 3. Core water content for alternative sets of interphase-friction correlations.

occur at mid-core (Fig. 2). The rapid, and prolonged, uncovering of the core in the prescribed slip case results in severe over-heating of the fuel rods, reaching 1200°C by 340 s (dashed line).

Predictions for the case using the TRAC interphase friction correlations (Run 4) are shown in Figs. 3 and 4, together with the results using the RELAP4/MOD6 correlations (Run 2) for comparison. The calculated time history of the core water content (Fig. 3) is very similar for each case. Both predict periodic uncovering and recovering of the core, until complete core uncovering around 390 s. This period of severe core uncovering is again reflected by the rapid rise in fuel-rod cladding temperature (Fig. 4) in each case. The peak cladding temperature is higher in the case using RELAP4 coefficients, since the core recovery predicted in the TRAC case (Run 4) at 415 s has not yet occurred. However, results not presented here show that accumulator injection, and consequent core recovery, is imminent after 450 s.

The final set of interphase-friction coefficients investigated, for the entire primary circuit, contains only the churn-turbulent and homogeneous regimes of the RELAP4/MOD6 correlations (Run 3). This study has been reported previously [2], but it is reported briefly here for completeness. The predicted time histories of core water content and mid-core cladding temperature, for the cases using the full RELAP4/MOD6 correlations (Run 2) and the partial set (Run 3), are shown in Figs. 5 and 6, respectively.

The predicted behaviour for the first 200 s of the transient is very similar in each case, typified by the core water content (Fig. 5). This is because only small regions of dispersed flow, for small periods of time, have been predicted so far, the flow being generally in the churn-turbulent regime. Subsequently, as more flow enters the dispersed-flow or transition-flow regimes, the behaviour of the core water content differs greatly. No core recovering occurs after 240 s for the case using the partial set of correlations (Fig. 5, dashed line).

The rises in mid-core cladding temperature (Fig. 6), corresponding to the periods of poor heat transfer to vapour, occur at different times in each case but the peak temperature is nearly the same, just below the cladding limit of 1200°C.

Reverse flow in the core produced the downturn in cladding temperatures, by displacing the greatly superheated vapour with much cooler vapour from the hot-leg and steam-generator.

4.3. *Effect of alternative representations of two-phase flow in the horizontal pipes*

The first aspect of the representation of stratified flow considered is the choice of interphase-friction

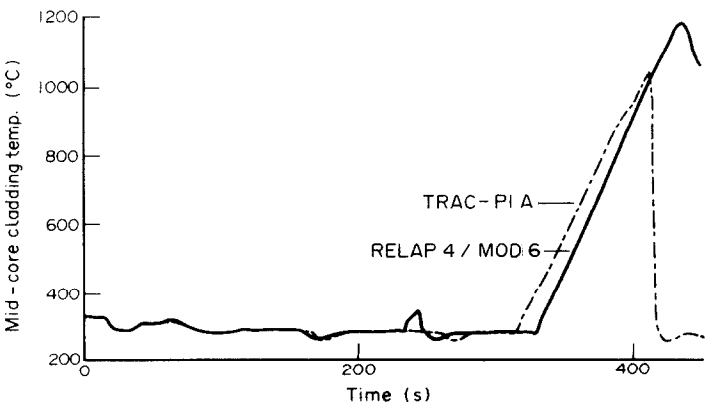

FIG. 4. Mid-core cladding temperature for alternative sets of interphase-friction correlations.

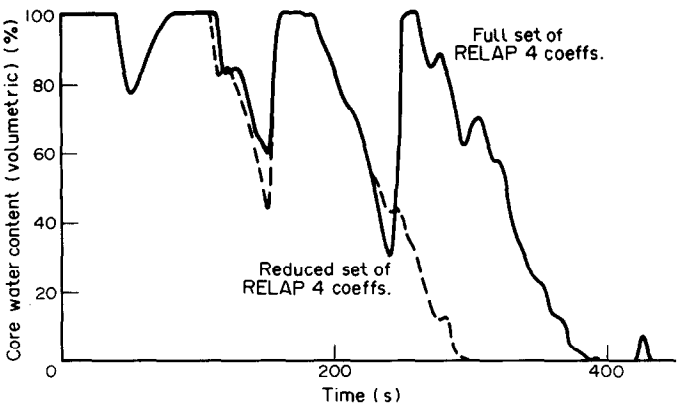

FIG. 5. Core water content for full and reduced RELAP4/MOD6 correlations.

correlation. Runs 5–7 cover a range of conditions, varying from homogeneous flow (Run 5), through dispersed flow (Run 6), to fully separated flow (Run 7). In each case the TRAC correlations were used in the rest of the primary circuit. The predicted time histories of core water content and cladding temperatures are shown in Figs. 7 and 8, respectively.

During the first 200 s of the transient, approximately, the behaviour of the primary coolant system shows little dependency on the interphase friction representation in the horizontal pipes. In particular, the core water content time histories (Fig. 7) for each case are in nearly exact agreement.

The behaviour of the fluid in the steam generators has a strong influence on the behaviour of the entire primary system for the remainder of the transient, i.e. 200–450 s. During periods of core uncovering, such as observed at 180, 205 and around 260 s (Fig. 7), the vapour which is being generated in the core prevents water from flowing around the system, via the cold-leg pipe and reactor downcomer, to refill the core; although there appears to be sufficient gravitational head for the refilling to occur. This is because a section of the steam generator hot side contains a slug of liquid, allowing little vapour to pass freely through the steam generator and hence preventing circulation in the primary system. Conditions at 310 s show this effect clearly (Fig. 11). Rapid core recovering occurs when vapour is able to pass freely through the steam generator, usually by succeeding in pushing the liquid slug over to the cold side of the steam generator.

The behaviour of the core water content over the period 250–450 s is seen to be greatly affected by the chosen interphase-friction representation in the horizontal pipes (Fig. 7). The homogeneous case, Run 5, shows an oscillatory emptying of the core from 250 to 340 s, the core remaining nearly totally empty of water from 340 s to the end of the calculation at 450 s. The mechanism for the observed oscillation in the core water content during the period 250–340 s appears to be as follows. A rapid decrease in the core water level results in less boiling in the core, the net effect being flow reversal of the vapour in the core and hot-leg pipe. The homogeneous conditions at the steam generator/hot-leg connection produce reversal of the liquid velocity at this point and consequently liquid drains from the steam generator into the hot leg. There is now a sufficient imbalance in gravitational head, considering the whole circuit, for a partial core recovery to occur. As the core recovers, the boiling rate in the core increases, returning the liquid from the hot leg back into the steam generator, restoring the gravitational balance (still with a partly-uncovered core). This process is repeated until the core is totally devoid of liquid at around 340 s.

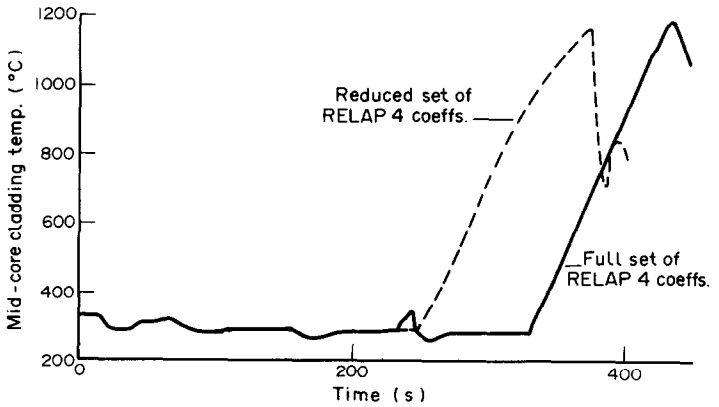

FIG. 6. Mid-core cladding temperature for full and reduced RELAP4/MOD6 correlations.

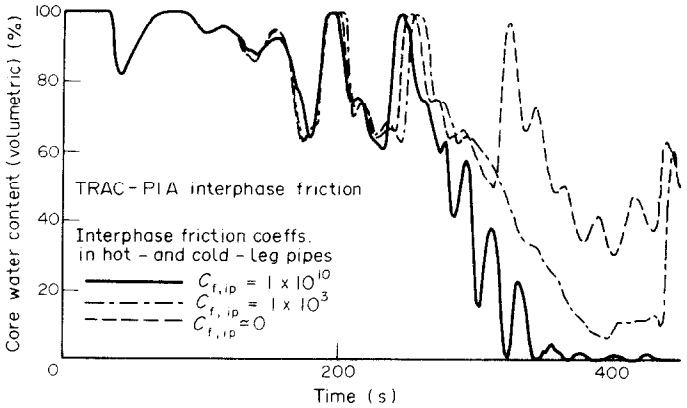

FIG. 7. Core water content for alternative representations of interphase friction in the horizontal pipes.

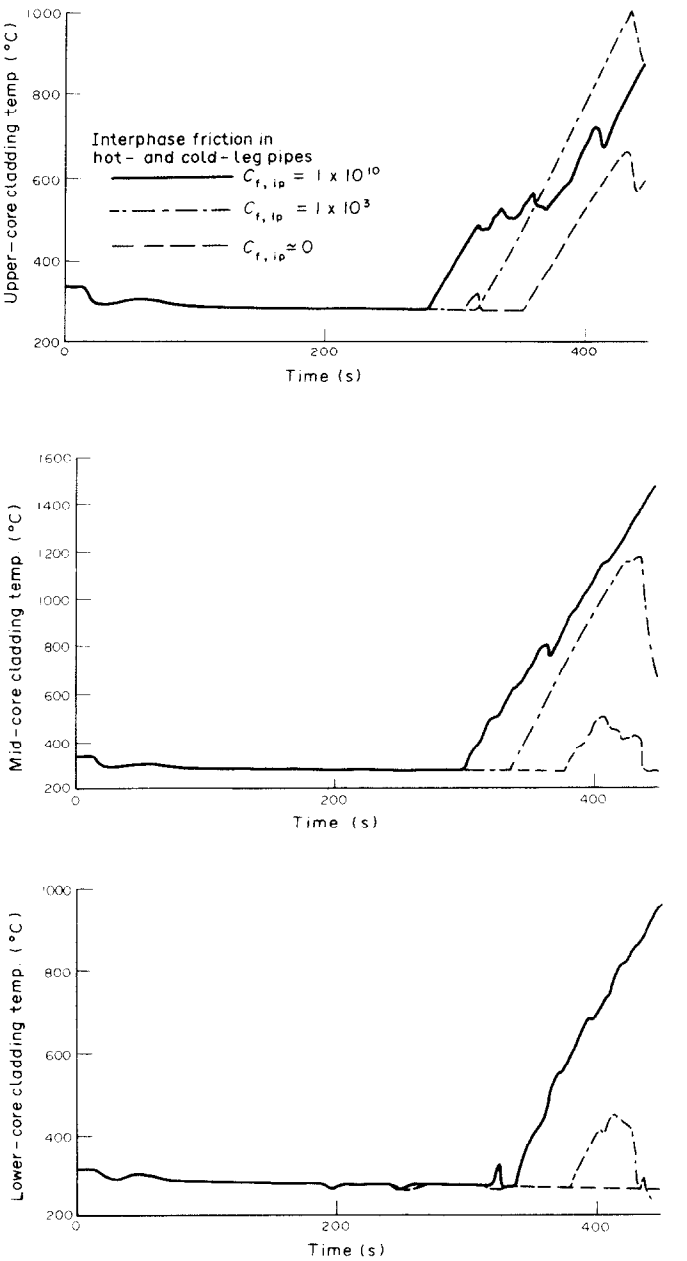

FIG. 8. Cladding temperatures for alternative representations of interphase friction in the horizontal pipes.

The calculation using a fixed interphase-friction coefficient, $C_{f,ip} = 10^3$ (Run 6), in the hot-leg pipe exhibits a slower emptying of the core (Fig. 7) than the homogeneous case. This is because the vapour, which is generated in the core, is able to pass into the steam generator, although not at a sufficient rate to allow core recovery. However, this vapour flow into the steam generator appears sufficient to prevent total core uncovering, approximately 10% of the core remaining covered during the severest part of the transient from 380 to 435 s.

The calculation which assumes a complete separation of phases in the horizontal pipes (Run 7), giving $C_{f,ip} \simeq 0$, shows very similar results to the previous case ($C_{f,ip} = 10^3$), until a rapid core recovering occurs around 320 s. This period of core recovering does not occur in the other two cases, and it ensures that a reasonable amount of water is present in the core throughout the transient. In Run 7, the liquid slug in the steam generator was destroyed around 320 s producing the core recovery. In the other two cases the slug remained, preventing core recovery at that time.

The effect of the various core water contents on the predicted fuel-rod cladding temperatures is shown in Fig. 8. The earlier, and more severe, uncovering predicted in the homogeneous case results in an early rise in cladding temperature throughout the core, and also gives a higher peak cladding temperature. The peak cladding temperatures obtained were 1470°C (homogeneous), 1180°C ($C_{f,ip} = 10^3$), and 650°C ($C_{f,ip} = 0$). Although the cladding temperature is still rising in the homogeneous case, it is not expected to rise substantially further since the accumulator trip is imminent.

The other effect that it is necessary to model in stratified flow is the influence of gravity on the liquid in the horizontal pipes, which will tend to spread the liquid along the pipe, and may form slugs. These effects, as detailed in Section 3.2, were included in Run 8, and the predictions compared against Run 7 in Figs. 9–12.

The core now does not experience the period of recovering which occurred previously around 320 s (Fig. 9). This is because the gravitational terms in the hot-leg pipe have spread liquid along the pipe from the steam generator, as may be seen in Figs. 11 and 12 (right-hand diagrams), reducing slightly the liquid inventory in the slug in the steam generator hot side. As a result it is less likely that the liquid slug will reach the top of the steam generator, thereby allowing core recovery. The long slug in the case without liquid-level terms (shown on the left-hand side) just reached the top of the steam generator by 310 s (Fig. 11), and core recovering subsequently occurred. However, in the other case, the slug just failed to reach critical height and eventually fell back, preserving substantial core voidage.

The core water content time histories are again reflected in the fuel-rod cladding temperatures (Fig. 10). The lack of full core recovering around 320 s allowed greater rises in cladding temperature, reaching 930°C in the upper core by 450 s. A peak cladding temperature of 650°C was predicted in the other case, neglecting the effects of interface level variations. Again, the accumulator injection was imminent by the end of the calculation, and one would expect the core recovering, which was already taking place by 450 s, to be rapidly completed.

4.4. *Effect of thermal non-equilibrium*

The effect of thermal non-equilibrium is shown for the core water content in Fig. 13. The reduced vaporization rates in the case of non-equilibrium is demonstrated by the shallower partial core uncovering predicted during the first 180 s. The major effect, however, is evident in the later stages of the transient. Two full core recoveries are predicted for the thermal equilibrium case (Run 8), but only one full core recovery occurs when thermal non-equilibrium is permitted (Fig. 13). This is due to the combination of reduced condensation rates in the steam generators, and reduced vaporization rates in the core, resulting in the removal of the plug of liquid in the steam generator hot side only once, around 220 s. The consequence of this is a somewhat deeper core uncovering, during the period 365–420 s, for the case with thermal non-equilibrium (Run 9).

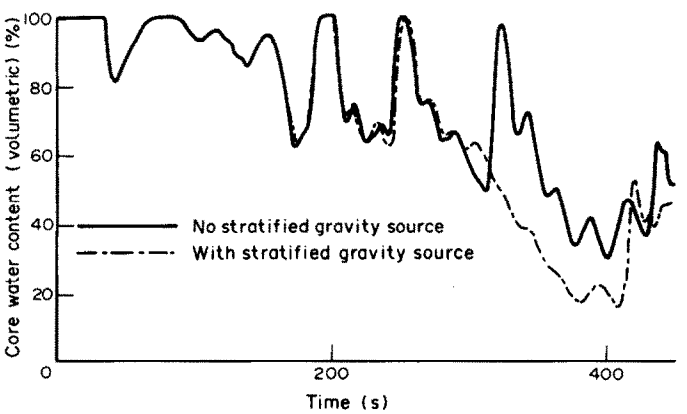

FIG. 9. Effect of interface level variation on core water content, for stratified two-phase horizontal flow.

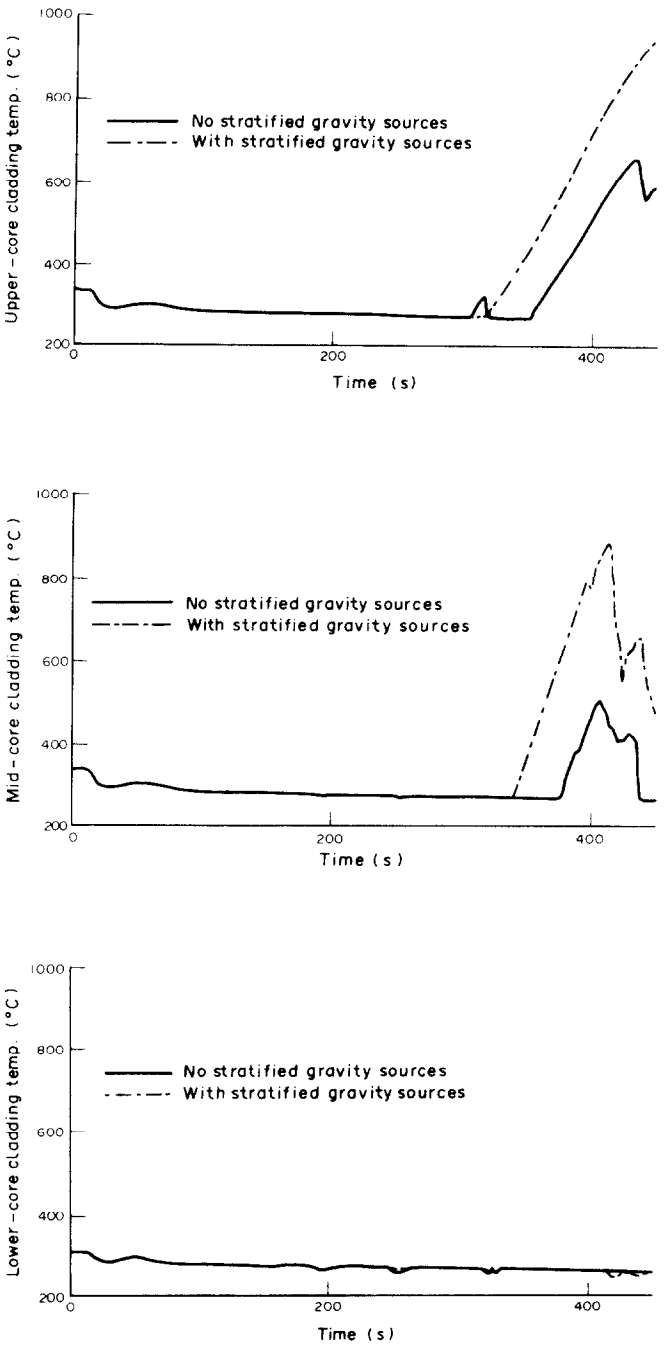

FIG. 10. Effect of interface level variation on cladding temperatures, for stratified two-phase horizontal flow.

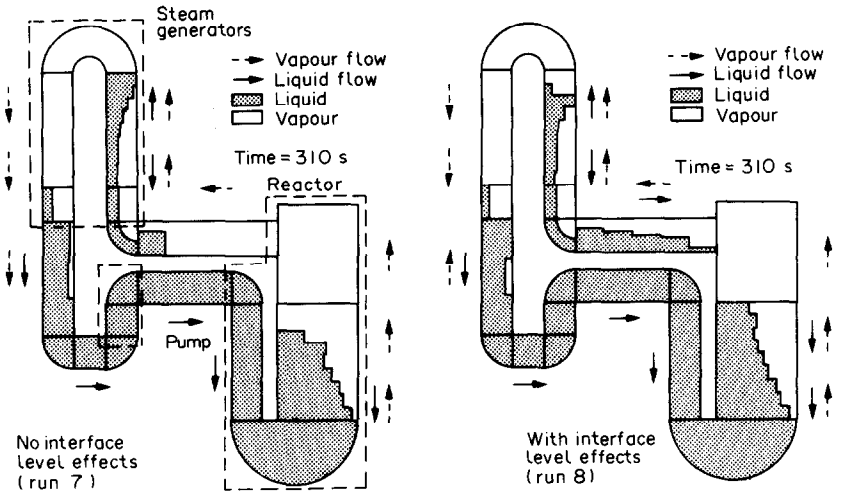

FIG. 11. Primary circuit liquid distribution after 310 s.

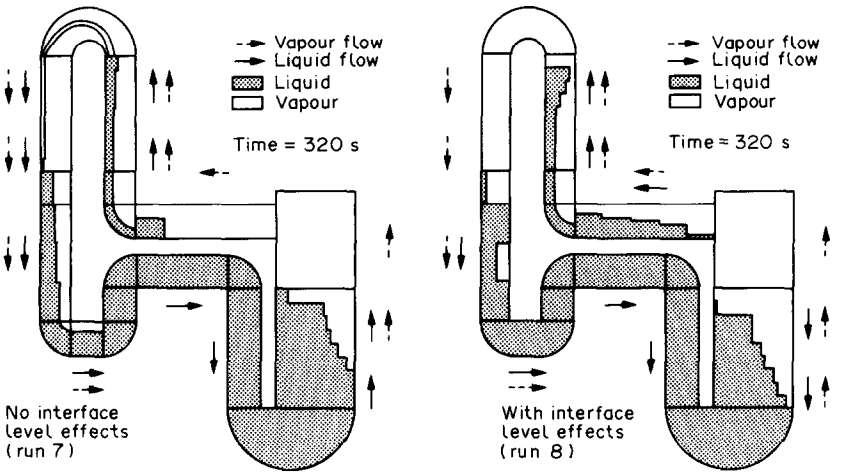

FIG. 12. Primary circuit liquid distribution after 320 s.

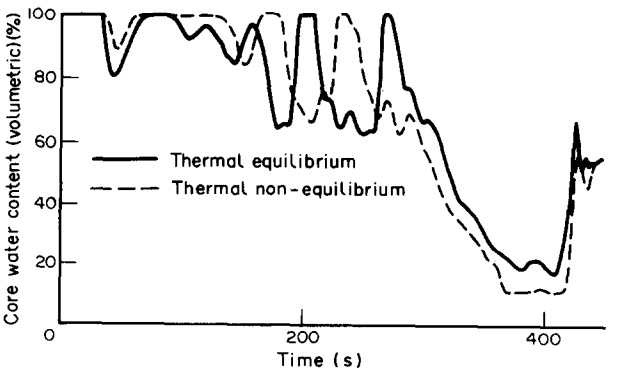

FIG. 13. Effect of thermal non-equilibrium on core water content.

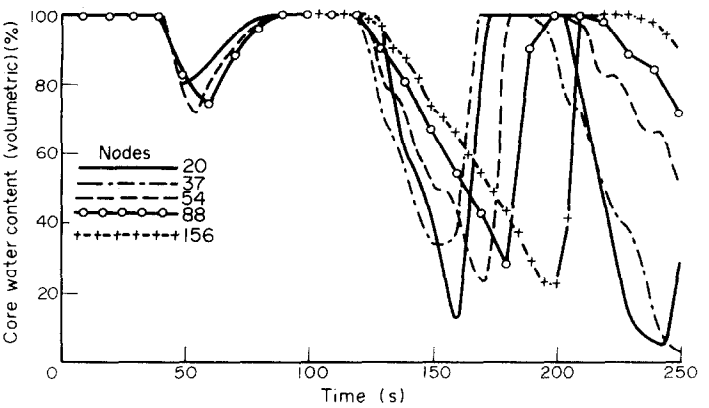

FIG. 14. Effect of nodalization on core water content.

The cladding temperatures (not shown here for space reasons) reflect the core water behaviour, giving peak cladding temperatures of 1144 and 930°C for the non-equilibrium and equilibrium cases, respectively.

4.5. *Effect of nodalization*

The core water content for 250 s of the transient, using grid distributions ranging from 20 to 156 nodes uniformly distributed (Runs 10–14), is shown in Fig. 14. The modelling of core heat transfer and interphase friction is simpler to that used for the calculations previously discussed, accounting for the deeper core uncovering around 160 s in these cases, and is described in ref. [2].

The effect of grid refinement is seen to be significant during the period of core uncovery around 150–200 s (Fig. 14). As more nodes are introduced, the period of core uncovery becomes more prolonged, although the depth of the uncovery shows little change. The cladding temperatures (not shown) are highest in the 156 node case (Run 14), due to this greatest period of core uncovery.

To investigate whether the nodalization of the core only has the most influence, a calculation has been performed which used the core nodalization of Run 14 (156 total nodes), with the rest of the circuit as for Run 12 (54 total nodes). The total number of nodes for this case was 72 (Run 15 in Table 3). Figure 15 presents the core water content for Runs 12, 14 and 15, again showing substantial lengthening of the period of core uncovery beginning around 120 s as more nodes are introduced. This indicates that grid refinement should not be confined solely to the core, and probably should be done throughout the circuit.

Further work, not shown here, indicates that approximately 450 nodes are required for grid independent predictions, and calculations employing up to 450 nodes will be finalized shortly. As has been shown, 88 nodes, and probably 156 nodes, are insufficient for grid independent solutions.

For each of the nodalizations considered, several runs were performed with various constant time-step sizes, to ensure negligible time-step effects in the nodalization study presented. For example, Fig. 16 shows the core water content for the 54 node grid using time steps of 0.1, 0.25, and 0.5 s. As may be seen there are no significant differences between the 0.1 and 0.25 s runs, but using a time step of 0.5 s leads to a loss of numerical accuracy. Hence a time step of 0.25 s was used for all 54 node grid runs.

4.6. *Computer-time requirements*

The computation time on a Perkin-Elmer 3220 mini-computer was 31 000 s (CPU) for a typical 54 node calculation, for 450 s of the transient.

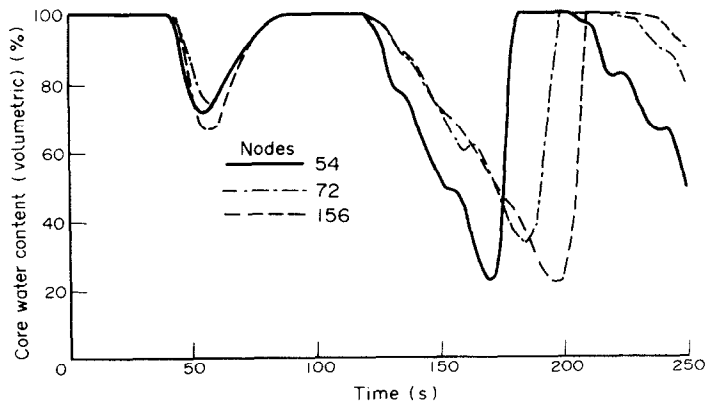

FIG. 15. Effect of selective nodalization on core water content.

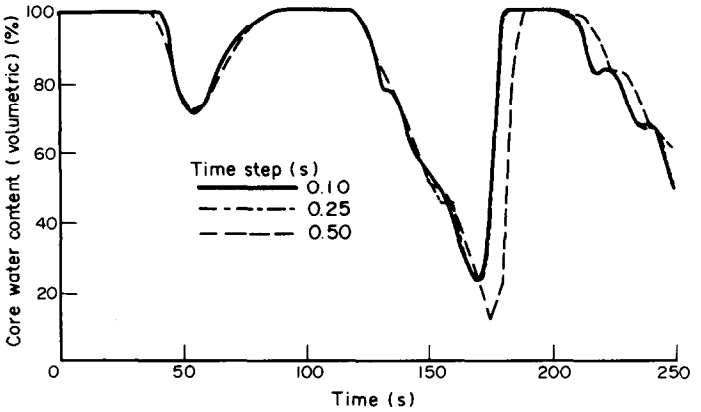

FIG. 16. Effect of time step size for a 54 node grid.

5. CONCLUSIONS

The conclusions may be summarized as follows:

(1) The predictions of the LAURA code are significantly affected by the chosen interphase friction correlations, at least for the particular accident selected for study.

(2) The representation of two-phase flow in the hot-leg pipes has a significant effect on the system behaviour. In particular, the assumption of homogeneous flow results in the greatest predicted fuel-rod cladding temperature (1470°C).

(3) Inclusion of gravitational effects in horizontal, stratified flow increases the predicted maximum cladding temperature from 650 to 930°C.

(4) The assumption of thermal non-equilibrium leads to a deeper core uncovery in the later stages of the transient, and consequently a greater peak cladding temperature.

(5) The effect of grid refinement is of the same order as the interphase-friction effects. For grid-independent predictions using LAURA, it has been shown that more than 88 nodes are required, and it is probable that in excess of 156 nodes are necessary. Further work, to be reported elsewhere, indicated that approximately 450 nodes are required for grid-independent predictions.

(6) Since other LOCA-analysis computer codes employ essentially the same mathematical principles as are embodied in LAURA, it may well be that their predictions are similarly sensitive to their numerical and physical input.

Acknowledgements—This work has been done under contract for H.M. Nuclear Installations Inspectorate. However, the views expressed in the paper are those of the authors and do not necessarily represent the views of the Inspectorate.

REFERENCES

1. J. F. Jackson, D. R. Liles, V. H. Ransom and L. J. Ybarrondo, *Nuclear Reactor Safety and Heat Transfer, Chap. 13—LWR System Safety Analysis* (edited by O. C. Jones). Hemisphere, Washington, DC (1981).
2. N. C. Markatos, S. M. Rawnsley and D. G. Tatchell, Analysis of a small break loss-of-coolant accident in a pressurised water reactor, *IMechE Conference Publications 1983–4, Heat and Fluid Flow in Nuclear and Process Plant Safety*, Paper C103/83, pp. 121–134 (1983).
3. TRAC-P1. *An Advanced Best-estimate Computer Program for PWR LOCA Analysis. Vol. 1: Methods, Models, User Information and Programming Details*, Los Alamos Scientific Laboratory Report LA-7279-MS, Vol. 1 (NUREG/CR-0063), June (1978).
4. RELAP4/MOD6. *A Computer Program for Transient Thermal-Hydraulic Analysis of Nuclear Reactors and Related Systems*, E. G. and G. Idaho Inc., January (1978).
5. W. L. Kirchner, Reflood heat transfer in a light water reactor, Ph.D. thesis, MIT Nuclear Engineering Department (1976).
6. S. R. M. Ellis and B. Gay, *Trans. Instn Chem. Engrs* 37 (1959).
7. TRAC-PD2: *An Advanced Best-estimate Computer Program for PWR LOCA Analysis*, Los Alamos Scientific Laboratory Report LA-8709-MS (1980).

APPENDIX 1

DESCRIPTION OF THE PROBLEM

A1.1. *Reactor-system geometry*

The configuration of the single-loop circuit and the model region diagram is shown in Fig. A1. The definition of each of the 14 regions shown, together with the main dimensions are given in Table A1.

Parts of the system such as the pressurizer, reactor upper head and emergency core cooling system (ECCS), which are separate from the primary circuit itself, are treated as control volumes external to the circuit, i.e. their interaction with the

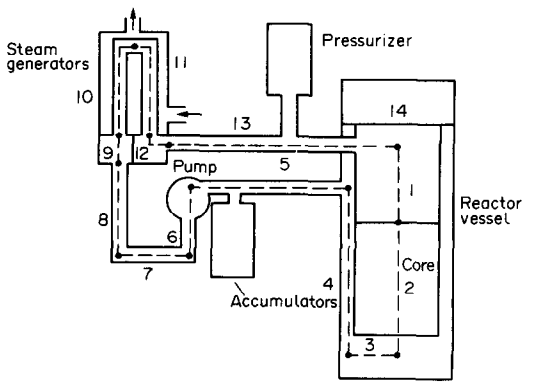

FIG. A1. Schematic configuration of the single-loop calculation domain.

Table A1. Definition of circuit regions

Region number	Component	Flow area (m^2)	Volume (m^3)
1	Reactor upper plenum	9.290	41.37
2	Core	7.169	26.21
3	Reactor lower plenum	4.859	29.62
4	Reactor downcomer	2.930	20.42
5	Cold-leg piping (pump to reactor)	1.533	9.63
6	Reactor pump	0.766	9.51
7, 8	Steam generator to reactor-pump piping	1.948	14.27
9	Steam generator outlet plenum	11.600	19.27
10, 11	Steam generator primary piping	3.968	83.26
12	Steam generator inlet plenum	11.600	19.27
13	Hot-leg piping (reactor to steam generator)	1.704	8.95
14	Reactor upper head	0.071	14.10

rest of the system is handled by the specification of appropriate boundary conditions for the circuit (Appendix 3).

A1.2. *Accident event sequence*

The postulated accident is caused by a 4 in. diameter break in the reactor lower plenum. On initiation of the break the system depressurizes, requiring (as seen) about 40 s to reach saturation conditions, at which time steam is first formed.

At 16 s after initiation the core is 'scrammed', reducing the core heat generation to about 10% of the full power over a period of 2 s, and diminishing to 3% of full power over the next 100 s. Ten seconds after the core 'scrams' the primary coolant pumps are tripped, decreasing the pump torque to zero after about 35 s. The first of the emergency core cooling systems is activated after 46 s, injecting high-pressure subcooled water into the system.

After approximately 450 s the system pressure was low enough for accumulator injection to begin.

APPENDIX 2

DERIVATION OF THE MOMENTUM SOURCE TERM DUE TO INTERFACE LEVEL VARIATION

The required momentum source term is obtained by integrating the hydrostatic force over the momentum control volume (dashed in Fig. A2), to derive the additional force acting on the liquid in the control volume. The vapour phase is removed from the analysis by using a reduced density for the liquid, equal to the liquid density minus the vapour density. Therefore, the vapour momentum equation requires no additional term.

The net force acting on the momentum control volume, due

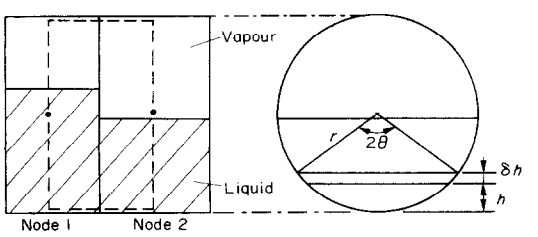

FIG. A2. Assumed flow pattern for stratified flow.

to the interface level variation, is given by

$$F_s = \int_1 p_h \, dA - \int_2 p_h \, dA, \tag{A1}$$

where p_h is the hydrostatic pressure, and A is the liquid cross-sectional area.

Considering the elemental area of height δh, shown in Fig. A2, the integrals on the RHS of equation (A1) are evaluated as follows.

Taking the bottom of the pipe as the pressure datum, the local hydrostatic pressure is given by

$$p_h = (\rho_l - \rho_g) g h, \tag{A2}$$

and the elemental area, δA, is given by

$$\delta A = 2r \sin\theta \, \delta h, \tag{A3}$$

therefore

$$\int p_h \, dA = \int 2(\rho_l - \rho_g) g h r \sin\theta \, dh. \tag{A4}$$

The local height h may be deduced from Fig. A2 as being

$$h = r(1 - \cos\theta), \tag{A5}$$

from which it follows by differentiation that

$$\delta h = r \sin\theta \, \delta\theta. \tag{A6}$$

Elimination of h and δh from equation (A4) gives

$$\int p_h \, dA = 2(\rho_l - \rho_g) g r^3 \int (1 - \cos\theta) \sin^2\theta \, d\theta. \tag{A7}$$

Now

$$\sin^2\theta = \tfrac{1}{2}(1 - \cos 2\theta), \tag{A8}$$

which simplifies equation (A7) as

$$\int p_h \, dA = (\rho_l - \rho_g) g r^3 \times \int (1 - \cos\theta - \cos 2\theta + \cos\theta \cos 2\theta) \, d\theta. \tag{A9}$$

Solution of equation (A9) is facilitated by the use of the relation

$$\cos\theta \cos 2\theta = \tfrac{1}{2}(\cos\theta + \cos 3\theta), \tag{A10}$$

giving

$$\int p_h \, dA = (\rho_l - \rho_g) g r^3 \times \int \left(1 - \frac{\cos\theta}{2} - \cos 2\theta + \frac{\cos 3\theta}{2}\right) d\theta. \tag{A11}$$

Integration of equation (A11) gives

$$\int p_h \, dA = (\rho_l - \rho_g) g r^3 \left[\theta - \frac{\sin\theta}{2} - \frac{\sin 2\theta}{2} + \frac{\sin 3\theta}{6}\right]. \tag{A12}$$

The limits of the integration are from $\theta = 0$ to θ_1, where $2\theta_1$ is the angle subtended at the centre of the pipe by the liquid level at node 1. Similarly for node 2, θ ranges from zero to θ_2.

Thus the final form of the required momentum source term is

$$F_s = (\rho_l - \rho_g) \frac{g r^3}{6} (6\theta_1 - 6\theta_2 - 3\sin\theta_1 + 3\sin\theta_2 - 3\sin 2\theta_1 + 3\sin 2\theta_2 + \sin 3\theta_1 - \sin 3\theta_2). \tag{A13}$$

Consideration of the pipe cross-sectional area filled by water yields a relationship between θ and the liquid volume fraction

$$\text{liquid area} = R_l \pi r^2 = \frac{r^2}{2}(2\theta - \sin 2\theta), \tag{A14}$$

giving

$$2\theta - \sin 2\theta = 2\pi R_l. \quad \text{(A15)}$$

Here θ is calculated by a Newton–Raphson iteration using equation (A15). Therefore, all the terms in the liquid momentum source term, equation (A13), are known.

For the calculation of wall friction, the liquid-pipe contact area is given by

$$A_{wl} = \left(\frac{2\theta}{\pi r}\right) \times \text{cell volume}. \quad \text{(A16)}$$

APPENDIX 3

BOUNDARY CONDITIONS AND PHYSICAL PROPERTIES

A3.1. *Boundary conditions*

A3.1.1. *Pressurizer.* At normal operating conditions the pressurizer vessel contains 30.59 m^3 of water and 20.39 m^3 of steam in equilibrium at a pressure of 15.52 MPa (344.8°C). The pressurizer is treated in the model as a constant volume vessel with no external heat transfer, i.e. isentropic. Solving equations for mass, entropy and volume continuity the pressurizer pressure is obtained, together with the masses of water and vapour present in the pressurizer. The mass flow of water or vapour leaving or entering the pressurizer is calculated from the pressure difference between the pressurizer and the hot-leg piping.

A3.1.2. *Pumped emergency coolant.* The total charging pump and high pressure injection system flow rate is 100 kg s^{-1} at a temperature of 38°C, initial injection occurring after 46 s. This is half the rated flow.

A3.1.3. *Reactor upper head.* The initial conditions for the upper head are: volume = 14.10 m^3; temperature = 323°C; saturation pressure = 11.93 MPa; liquid density = 656 kg m^{-3}; and fluid mass = 9249.6 kg.

The modelling of the upper head is identical to that of the pressurizer vessel, i.e. a constant-volume vessel with no external heat transfer.

A3.1.4. *Treatment of break.* The mass flow through the reactor lower plenum break is taken to be linearly proportional to the pressure difference across the break, the constant of proportionality being such as to give the same initial break flow rate as in an unpublished RELAP4 4 in. break calculation.

A3.1.5. *Steam generator heat transfer.* The heat-transfer rate between the primary and secondary fluids in the steam generator is calculated from the primary–secondary temperature difference and, for the present, a constant heat-transfer coefficient of 1.26×10^8 W m^{-2} K^{-1}. This value gives the correct steady-state heat-transfer rate.

For the calculations presented here the steam generator secondary temperature is prescribed as shown in Fig. A3(a). However, recent LAURA calculations predict the secondary temperature.

A3.1.6. *Core heat generation.* A given time history for the core heat generation is used [Fig. A3(b)]. The total initial core heat-generation rate is 3479.2 MW partitioned axially in the core in the ratio 0.268 : 0.464 : 0.268.

A3.2. *Physical properties*

A3.2.1. *Density.* The *liquid* density for saturation conditions

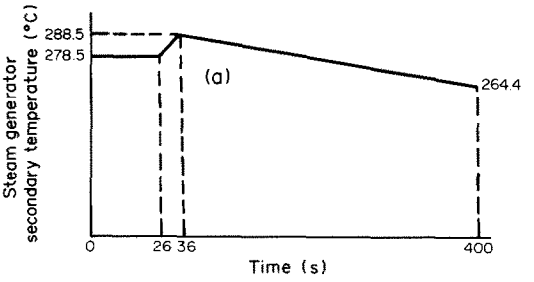

FIG. A3(a). Steam generator secondary fluid temperature.

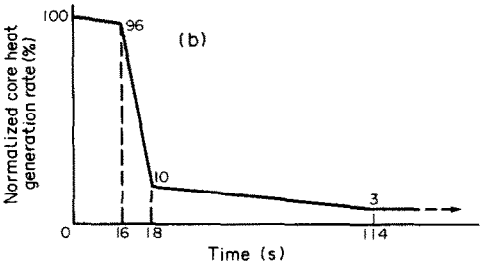

FIG. A3(b). Normalized core heat generation rate (percentage of normal operating power).

is obtained from property tables

$$\rho_l = \min\left(958.0, \frac{1.0706 \times 10^4}{p^{0.17464}}\right) \text{kg m}^{-3}. \quad \text{(A17)}$$

Equation (A17) is accurate to within 8% over the range: 10^5 Pa $\leqslant p \leqslant 1.6 \times 10^7$ Pa. For subcooled liquid, ρ_l is taken as the saturation density at the liquid temperature, since $\partial\rho/\partial p$ at constant temperature is small (< 2%). For the vapour density, the following expression is obtained from property tables, accurate to within 10% over the shown range of pressure

$$\rho_g = 9.22 \times 10^{-6} p^{0.959}, \quad 10^5 \text{ Pa} \leqslant p \leqslant 1.6 \times 10^7 \text{ Pa}. \quad \text{(A18)}$$

A3.2.2. *Saturation enthalpy.* The following relation, accurate to within 4% over the same range of pressure as in equation (A17), is used for *liquid*

$$h_{s,l} = 1.8278 \times 10^4 p^{0.27126} \text{ J kg}^{-1}, \quad \text{(A19)}$$

for *vapour*

$$h_{s,g} = 2.8095 \times 10^6 - 8.37 \times 10^{-10} p^2, \quad \text{(A20)}$$

$$3 \text{ MPa} \leqslant p \leqslant 15.5 \text{ MPa}.$$

A3.2.3. *Fuel rods.* Uniform conductivity and volumetric specific heat are assumed for the rods, equal to 4.0 W m^{-1} K^{-1} and 1.031×10^6 J m^{-3} K^{-1}, respectively. The modelling also considers the clad and the gap between rods and clad, with the following property values.

Gap: conductivity = 0.72 W m^{-1} K^{-1};

specific heat = 1.552 J m^{-3} K^{-1}.

Clad: conductivity = 16.0 W m^{-1} K^{-1};

specific heat = 6.21×10^5 J m^{-3} K^{-1}.

Cladding deformation effects are not included.

TRANSFERT THERMIQUE PENDANT L'ACCIDENT DE PERTE DE REFRIGERANT PAR UNE FISSURE DANS UN REACTEUR A EAU PRESSURISEE—UNE ETUDE PARAMETRIQUE

Résumé—Une question importante de sécurité dans la conception de réacteur à eau pressurisée (PWR) est l'accident de perte de réfrigérant (LOCA) dans lequel une fissure dans le circuit réfrigérant primaire conduit à la dépression, à l'ébullition du réfrigérant, à la réduction du refroidissement du coeur du réacteur et, malgré les opérations nécessaires, à la surchauffe des barres de combustible. Cette éventualité a conduit à l'élaboration de plusieurs modèles d'analyse de sûreté, dont la validité ne peut être connue qu'après avoir soumis leur précision et leur sensibilité à des études paramétriques telles que: études nodales pour s'assurer que les résultats sont indépendants du maillage; étude sur l'entrée empirique alternative telle que les représentations du transfert thermique, le choix des régimes d'écoulement etc...., et la représentation de l'écoulement diphasique stratifié dans les tubes horizontaux. On présente ici de telles études paramétriques pour un accident sur PWR. Les résultats sont présentés et discutés. On constate que les calculs sont sensiblement affectés par les noeuds de maille utilisés, par le choix des formules de transfert thermique et de frottement à l'interphase et par modélisation de l'écoulement diphasique dans les tubes horizontaux. De telles sensibilités peuvent être révélées par d'autres simulations LOCA.

DER WÄRMEÜBERGANG WÄHREND EINES KÜHLMITTELVERLUSTUNFALLS MIT KLEINEM LECK—EINE PARAMETERSTUDIE FÜR EIN 100 cm-LECK IM UNTEREN PLENUM

Zusammenfassung—Ein wichtiger Sicherheitsaspekt bei der Berechnung von Druckwasserreaktoren (PWR) ist ein Kühlmittelverlustunfall (LOCA), bei dem ein Rohrbruch im Primärkreislauf einen Druckabfall verursacht, der zum Sieden des Kühlmittels, damit zur verminderten Kühlung des Reaktorkerns und, sofern keine Abhilfemaßnahmen getroffen werden, zur Überhitzung der Brennstäbe führt. Dieser Aspekt hat zur Entwicklung einiger Computermodelle für die Sicherheitsanalyse geführt, deren Gültigkeit erst abgeschätzt werden kann, nachdem ihre Genauigkeit und Empfindlichkeit parametrischen Studien unterzogen wurde, wie: Diskretisierungsstudien, um die Unabhängigkeit der Ergebnisse von der gewählten Gitterstruktur zu gewährleisten, die Untersuchung alternativer empirischer Berechnungsunterlagen wie Wärmeübergangsbeziehungen, Wahl der Strömungsformen und Darstellung der geschichteten Zweiphasenströmung in den waagerechten Rohren. Die vorliegende Arbeit berichtet über solche Parameterstudien für einen angenommenen Unfall in einem Druckwasserreaktor. Die Ergebnisse werden vorgelegt und diskutiert. Es zeigt sich, daß die Berechnungen beträchtlich von der verwendeten Anzahl der Gitterpunkte abhängen, ebenso von den gewählten Wärmeübergangs- und Reibungskorrelationen für die Phasengrenzflächen und von der Modellierung der geschichteten Zweiphasenströmung in waagerechten Rohren. Diese Empfindlichkeiten dürften, darauf wird hingewiesen, auch bei anderen Simulationen des Kühlmittelverlustunfalls festgestellt werden.

ТЕПЛОПЕРЕНОС ПРИ НЕБОЛЬШОЙ АВАРИЙНОЙ УТЕЧКЕ ТЕПЛОНОСИТЕЛЯ ИЗ ВОДООХЛАЖДАЕМОГО РЕАКТОРА—ПАРАМЕТРИЧЕСКОЕ ИССЛЕДОВАНИЕ АВАРИИ С ОБРАЗОВАНИЕМ ЧЕТЫРЕХДЮЙМОВОЙ ТРЕЩИНЫ В НИЖНЕЙ КАМЕРЕ ПОВЫШЕННОГО ДАВЛЕНИЯ

Аннотация—При проектировании реакторов, охлаждаемых водой под давлением, особое внимание обращается на меры безопасности на случай аварии с утечкой теплоносителя. В результате разрыва основного контура с теплоносителем давление резко снижается, теплоноситель закипает (из-за недостаточного охлаждения активной зоны реактора) и, если не приняты специальные меры, топливные стержни сильно перегреваются. Значимость проблемы обусловила разработку ряда расчетных моделей для анализа эксплуатационной безопасности. Их точность и надежность можно оценить только после проведения соответствующих параметрических исследований: способа построения узловых точек, при котором используемые результаты не влияют на выбор сетки; возможности использования других эмпирических входных данных, например, по теплопереносу, режимам течения и т.д., и стратифицированного двухфазного течения в горизонтальных трубах. В работе проводятся такие параметрические исследования для случая смоделированной аварии реактора, охлаждаемого водой под давлением. Представлены полученные результаты и проведено их обсуждение. Сделан вывод о том, что результаты расчетов сильно зависят от числа узлов сетки, от используемых зависимостей по теплопереносу и межфазному гидравлическому сопротивлению, а также от способа моделирования стратифицированного течения в горизонтальных трубах. Высказано предположение, что такая же зависимость результатов может наблюдаться и при других способах моделирования случаев утечки теплоносителя.